Surface & Coatings Technology 203 (2009) 3278–3285

Contents lists available at ScienceDirect

Surface & Coatings Technology

journal homepage: www.elsevier.com/locate/surfcoat

# Rumpling of CVD (Ni,Pt)Al diffusion coatings under intermediate temperature cycling

V.K. Tolpygo [1], D.R. Clarke *

*Materials Department, College of Engineering, University of California, Santa Barbara, CA 93106-5050, United States*

ARTICLE INFO

*Article history:*
Received 25 November 2008
Accepted in revised form 8 April 2009
Available online 20 April 2009

*Keywords:*
Rumpling
Cyclic oxidation
Aluminide
Superalloy

ABSTRACT

The development of surface undulations during cyclic oxidation of diffusion (Ni,Pt)Al coatings on second generation nickel-base superalloys, the phenomenon of "rumpling," represents one of the major forms of coating degradation during service at high temperatures. Previous studies of the phenomenon have invariably involved cycling between a high temperature, typically 1150 °C, and room temperature, or close to it (~50–100 °C). In this work, we show that most of the rumpling occurs on thermal cycling in a narrow temperature range between 1150 °C and a lower temperature of about 1000 °C. Furthermore, there is little difference in the rumpling amplitude when the lower temperature is reduced below 1000 °C, even down to room temperature, suggesting that the mechanisms responsible for rumpling operate principally at temperatures above 1000 °C. These results have important implications for the viability of various mechanisms proposed for rumpling as well as for life prediction models.



## 1. Introduction

Platinum-modified diffusion nickel aluminide coatings are widely used to protect nickel-based superalloy components, such as high-pressure turbine blades and nozzles, from oxidation and hot corrosion. They are also one of the types of metallic coatings used as bond-coats when the components are over-coated with thermal barrier coatings. It is now well established that platinum-modified diffusion aluminide coatings are susceptible to the development of surface undulations when thermally cycled at elevated temperatures [1–4], and that this can lead to premature coating failure during service. The coating degradation can take the form of cracking and spallation of the protective oxide scale along the rumpled ridges and accelerated oxidation as well as local separations and delamination of thermal barrier coatings when they are deposited on the aluminide coating [2].

In standard furnace cycling tests, coated superalloy buttons are thermally cycled between an oxidation temperature, $T_1$, and room temperature, or close to it. Alternatively, coated superalloy bars are subject to repeated exposure to a hot flame in a burner-rig test with forced air cooling between each flame exposure. These tests are meant to reproduce the behavior of the coatings under representative use conditions, for example upon turning the turbine on and off, or switching between maximum power and some intermediate power level. As far as we are aware, all the previous studies of the rumpling phenomenon in aluminide coatings have been performed by thermal cycling between room temperature and the oxidation temperature. The key parameters of such tests are the number of cycles, the oxidation temperature, $T_1$, and the dwell time per cycle at the oxidation temperature, $T_1$. In this work, we have explored yet another factor, the lower temperature segment, $T_2$, of the thermal cycle. The major objective of these experiments is to determine the effect of the temperature regime, specifically, the magnitude of the temperature difference $\Delta T = T_1 - T_2$ in each cycle, on the rumpling of an aluminide coating. As will be shown, the results also severely constrain possible explanations for the rumpling phenomenon.

The approach we have adopted in these experiments was to fix the oxidation temperature, $T_1 = 1150$ °C, the total number of cycles ($N = 100$), and the dwell time at 1150 °C (1 h per cycle), while selecting different lower temperatures, $T_2$, for each sequence of 100 cycles. Although many other combinations of $T_1$, $T_2$ and dwell time can be considered, this temperature regime was chosen as it provides a direct comparison with the majority of the previous studies of rumpling, which involved cycling between oxidation temperature and room temperature.

## 2. Experimental details

The (Ni,Pt)Al coatings examined in this work were supplied by Howmet Castings (Whitehall, MI). They were produced by a low-aluminum activity CVD aluminizing of platinum-plated disk-shape buttons of René N5 superalloy. The specimens, about 25.4 mm in diameter and 3.1 mm thick, the standard configuration in furnace cycle tests, were studied in both their as-aluminized condition and after polishing to remove ridges on the coating surface, as described previously [3,4]. The outer part of the coating, approximately 40 μm thick, consisted of a single-phase layer of nickel-rich aluminide (Fig. 1). The average chemical composition of this outer layer,

* Corresponding author. School of Engineering and Applied Sciences, Harvard University, Cambridge, MA 02138, United States. Tel.: +1 805 893 8275.
*E-mail address:* clarke@seas.harvard.edu (D.R. Clarke).
[1] Now at Honeywell Aerospace, Phoenix, AZ, United States.

0257-8972/$ – see front matter © 2009 Elsevier B.V. All rights reserved.
doi:10.1016/j.surfcoat.2009.04.016

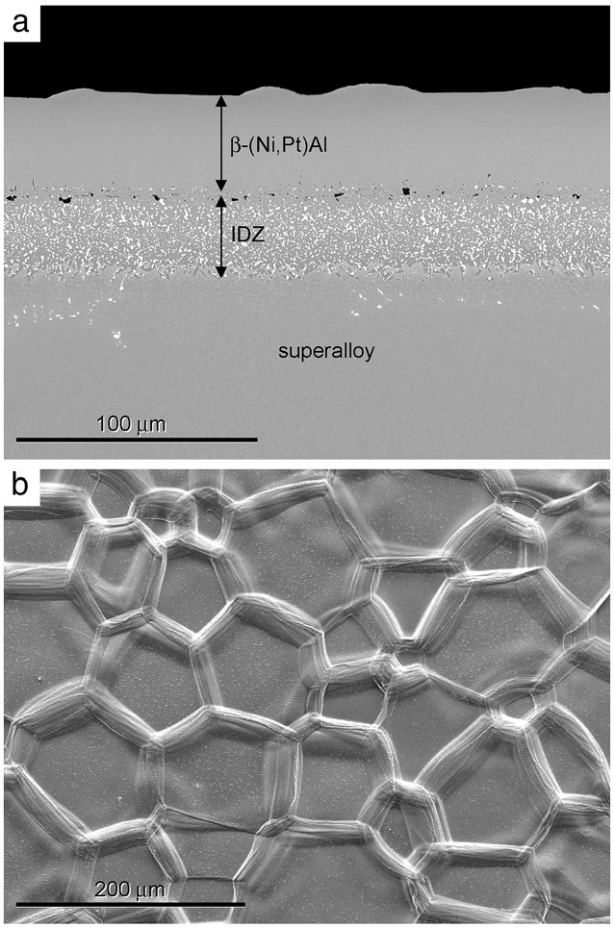


**Fig. 1.** Cross-section (a) and surface (b) microstructures of the as-deposited platinum–aluminide diffusion coating on René N5 superalloy. The single-phase outward-grown portion of the coating, β-(Ni,Pt)Al, and the inter-diffusion zone (IDZ) are indicated.

measured on polished cross sections by EDX, is presented in Table 1. Because the composition varied across the coating thickness (for aluminum, for example, from 45 at.% near the surface to about 36 at.% at the interface between the outer layer and the inter-diffusion zone), the concentrations were averaged over the entire outward-grown portion of the coating. All the buttons were cut from the same single-crystal superalloy bar and coated in a single batch to ensure that the rumpling results of different experiments are as comparable with each other as possible. (As previous studies show, chemical composition of the coating and the superalloy [1,5], as well as the coating thickness [1,6] have an effect on rumpling.) All other relevant details of the coating chemistry and microstructure, as well as the characterization methods have been reported recently [3–5].

The cyclic oxidation experiments were carried out using an automatic rig that moved the specimens between two adjacent

**Table 1**
Average chemical compositions of the outer layer and compositions of individual phases in the (Ni,Pt)Al coating in as-processed condition and after 100 one-hour cycles at 1150 °C in air measured by EDX (at.%).[a]

| Coating specimen | | Al | Cr | Co | Ni | Mo | Ta | W | Pt |
|---|---|---|---|---|---|---|---|---|---|
| As-processed: average | | 39.8 | 3.5 | 4.2 | 45.0 | 0.1 | 0.3 | 0.1 | 7.0 |
| After 100 h at | Average | 30.1 | 5.2 | 5.2 | 53.8 | 0.2 | 0.7 | 0.1 | 4.7 |
| 1150 °C | β phase[b] | 30.3 | 5.2 | 5.1 | 53.7 | 0.1 | 0.7 | 0.1 | 4.8 |
| | Isolated γ′ grains | 20.2 | 4.3 | 6.3 | 62.3 | 0.5 | 2.6 | 0.5 | 3.3 |
| | γ′ layer in mid-section | 20.3 | 3.8 | 6.3 | 62.1 | 0.6 | 3.0 | 0.6 | 3.3 |

[a] Trace amounts of Re in the coating were not quantified because of an overlap with tungsten EDX peaks.
[b] Beta-phase undergoes martensitic transformation during cooling to room temperature.

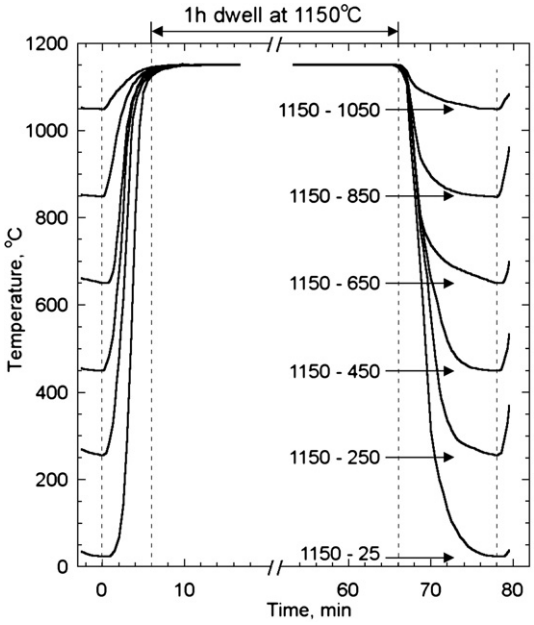


**Fig. 2.** Typical temperature–time profiles during cyclic oxidation for several different lower temperatures $T_2$.

horizontal tube furnaces. One of the furnaces was held at the oxidation temperature, $T_1 = 1150$ °C. The other furnace was used for cooling the specimens down to temperature $T_2$ selected in the range from 250 °C to 1050 °C. Each test consisted of 100 uninterrupted cycles with one-hour exposure at 1150 °C in ambient air, cooling to temperature $T_2$ and heating back to 1150 °C. There was essentially no dwell time at the lower temperature, so the next heating segment started immediately upon reaching the lower temperature $T_2$ (Fig. 2). In these experiments, all thermal cycles (except for the first and the last) were conducted between $T_1$ and $T_2$. As shown in Fig. 2, the heating and cooling rates in these experiments were similar although not the same, a factor which may affect the cyclic behavior of the coating.

For comparison, one specimen was subject to 100 cycles with a long dwell time at $T_2$. In this experiment, thermal cycling was between 1150 °C and 950 °C ($\Delta T = 200$ °C), with a one-hour dwell at both 1150 °C and 950 °C. Another test was performed using the "standard" cyclic regime, when the specimens were cooled to room temperature in each cycle. An additional experiment consisted of 100 one-hour cycles between 1200 °C and room temperature followed by another set of 100 one-hour cycles between 1100 °C and room temperature. The goal of this test was to evaluate rumpling behavior at lower $T_1$ of a coating that has already developed substantial surface roughness. Finally, two separate specimens, one in the as-aluminized condition and one polished, were isothermally oxidized at 1150 °C for 100 h.

The coating surface roughness of all the specimens after 100 cycles was measured using an optical interferometer, as described previously [5]. In this report, two key rumpling parameters, the root-mean-square roughness ($R_q$) and the average wavelength ($W$) are presented. The root-mean-square roughness, defined in the usual way, is a direct output of the interferometer. The average wavelength was determined as $W = 2\pi R_q \Delta^{-1}$ where $\Delta$ is the root-mean-square slope of the surface.

## 3. Results

To place the results presented in this contribution in perspective, the progressive rumpling of the (Ni,Pt)Al coating surface during the "standard" cyclic test between 1150 °C and room temperature with a

one-hour dwell at 1150 °C is shown in Fig. 3. In the figure, both the root-mean-square roughness and the average wavelength are shown as a function of the number of cycles. In this test, the as-aluminized coating was exposed to 200 cycles, and the roughness parameters were repeatedly measured at room temperature after a prescribed number of cycles to illustrate the continuous evolution of $R_q$ and $W$ with oxidation time. The error bars in Fig. 3 indicate the standard deviation of 10 individual measurements on one specimen covering a total surface area of about 10 mm$^2$.

The major findings of the cyclic oxidation tests with different lower cycle temperature $T_2$ are shown in Fig. 4. Each test is represented by a single data point indicating surface roughness of the coating after 100 cycles for a given temperature $T_2$. Note that the dashed lines in Fig. 4 are guides for eye only, so they do not imply a functional dependence of $R_q$ vs. $T_2$. The spread of the roughness data for different tests probably reflects natural variability of the rumpling and may also be related to some differences in the heating and cooling rates between the tests. Nevertheless, there appears to be a statistically significant slope of the $R_q$ values with increasing $T_2$ in the range between room temperature and about 1000 °C.

The results in Fig. 4 demonstrate that the amplitude of rumpling, which is proportional to $R_q$, does not increase with increasing $\Delta T$. Furthermore, the regular cyclic regime between 1150 °C and room temperature produces slightly less rumpling than other tests with a much smaller $\Delta T$, for example after cycling between 1150° and 950 °C. Most surprisingly, the surface roughness after thermal cycling between 1150° and 1050 °C ($\Delta T = 100$ °C) is no less than after other tests with much larger $\Delta T$. As seen in Fig. 4, the same behavior was found for both the as-aluminized coating as well as the polished coating, although all the $R_q$ values for the polished surfaces are consistently smaller. Also shown in Fig. 4 are the results of isothermal oxidation for the same hot time (100 h) at 1150 °C and the initial roughness for both groups of specimens before oxidation. In agreement with the previously published data [4,7], isothermal oxidation does increase surface roughness of (Ni,Pt)Al coatings, but it is much smaller than after cyclic oxidation.

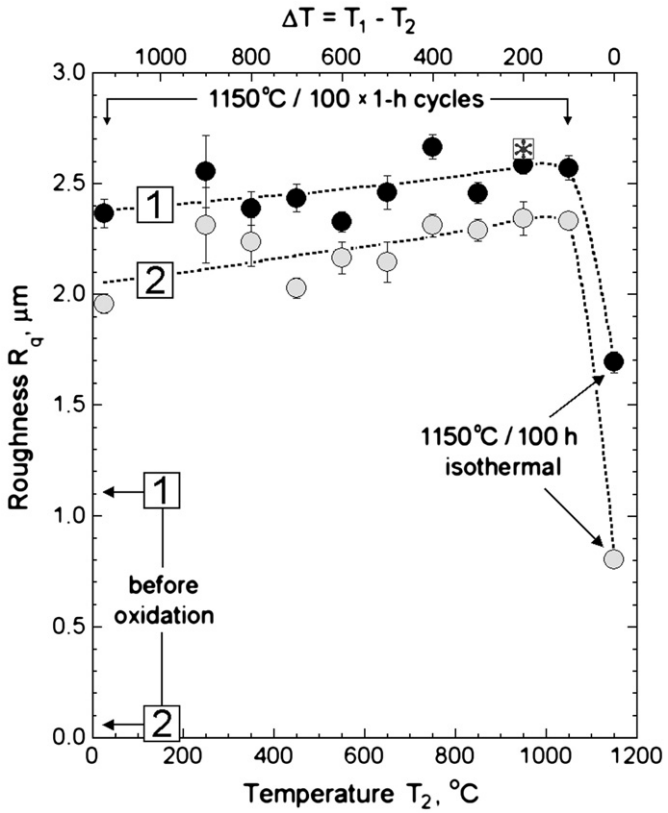


**Fig. 4.** Root-mean-square roughness $R_q$ of the (Ni,Pt)Al coating surface after 100 one-hour cycles at 1150 °C as a function of lower cycling temperature, $T_2$. The results for as-aluminized coating (1) and polished coating (2) are shown by the solid and open symbols, respectively. For comparison, the $R_q$ value after 100 cycles between 1150 °C and 950 °C with one-hour dwell time at both temperatures is indicated by the asterisk. For further comparison, the results after isothermal oxidation at 1150 °C for 100 h and the initial values of $R_q$ before oxidation are also shown. The dotted lines through the data are guides to the eye.

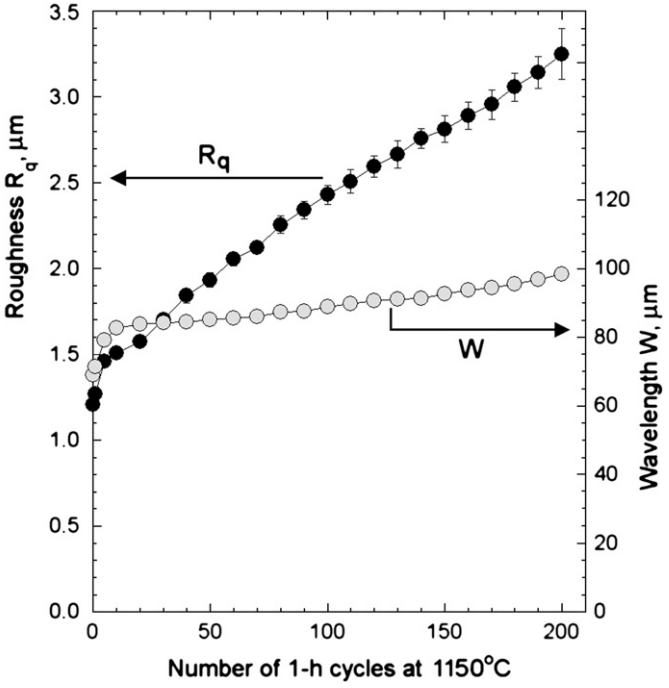


**Fig. 3.** Rumpling evolution of the (Ni,Pt)Al coating surface during cyclic oxidation between room temperature and 1150 °C (one-hour cycles) showing root-mean-square roughness (solid symbols, left axis) and calculated effective wavelength (open circles, right axis) as a function of oxidation time.

To illustrate the effect of dwell time at temperature $T_2$, one specimen was cycled between 1150° and 950 °C but with a hold of 1 h at both temperatures. The resulting $R_q$ value is shown by the asterisk symbol in Fig. 4. Comparing with the matching test with a very short dwell at $T_2$ (the solid circle at 950 °C in Fig. 4), it can be concluded that only a very small increase of $R_q$ is achieved by using prolonged exposures at the lower cycle temperature. Indeed, the magnitude of $R_q$ after the test with one-hour dwell is merely 3% higher than after the test with 1–2 min dwell at 950 °C.

The average rumpling wavelength, shown in Fig. 5, is even less sensitive to the value of the lower temperature, $T_2$, but there is nonetheless a clear systematic difference between cyclic and isothermal exposures, as reported previously [4,5]. Somewhat surprisingly, the wavelengths after cyclic oxidation of the polished specimens are consistently longer than of the as-aluminized specimens. This may be attributed to some geometrical differences between surface undulations. For example, the polished coating develops predominantly grain boundary grooves, as opposed to grain boundary ridges on the as-aluminized coating [3,4].

The apparent insensitivity of the rumpling amplitude (Fig. 4) and wavelength (Fig. 5) on the magnitude of $\Delta T$ during cyclic oxidation (for $\Delta T > 100$ °C or so) suggests that all the mechanisms responsible for rumpling operate primarily within a relatively narrow temperature range between $T_1$ (1150 °C in these tests) and approximately 1050 °C. Cooling down to lower temperatures in each cycle does not produce any further increase of the rumpling.

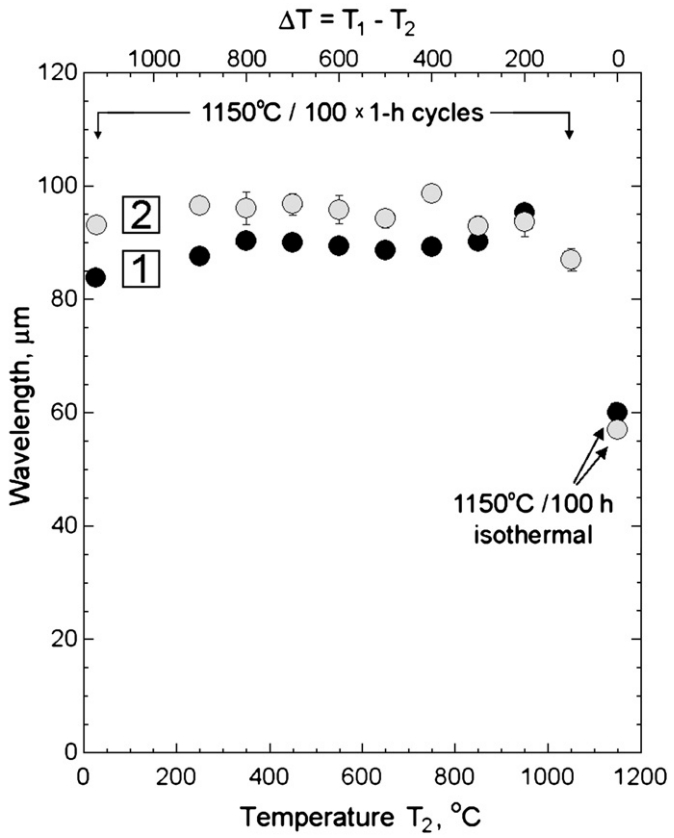


**Fig. 5.** Effective wavelength, $W$, of the (Ni,Pt)Al coating surface after 100 one-hour cycles at 1150 °C as a function of lower cycling temperature, $T_2$. The results for as-aluminized coating (1) and polished coating (2) are shown by the solid and open symbols, respectively.

Fig. 6 shows the results of the two-stage experiment, in which a polished specimen was given 100 one-hour cycles at 1200 °C followed by another 100 one-hour cycles at 1100 °C. In both cases, the specimen was cooled to room temperature in each cycle. As our previous study demonstrated [7], rumpling rate of the same coatings during cyclic oxidation at 1200 °C is much higher than at 1150 °C, but it is very low at 1100 °C. It might seem reasonable to assume that the strong temperature dependence simply reflects the fact that various diffusion-controlled processes, such as aluminum depletion and oxide thickening, occur much slower at 1100 °C, resulting in a lower rumpling rate than at higher oxidation temperatures. So, the purpose of the present two-stage experiment was to generate an extensively rumpled coating, in which all the processes that presumably drive rumpling are already operating, and determine whether they continue to operate at lower $T_1$. The results in Fig. 6 reveal a dramatic decrease of the rumpling rate when temperature $T_1$ is reduced from 1200° to 1100 °C. Furthermore, the rumpling rate at the second stage in Fig. 6, $dR_q/dt \approx 2.0\times10^{-3}$ μm/h, is similar to that observed on a "fresh" (unexposed) coating upon cycling at 1100 °C, $dR_q/dt \approx 2.2\times10^{-3}$ μm/h [7]. In other words, all the changes in the coating that have occurred during the 100 cycles at $T_1 = 1200$ °C essentially have no effect on rumpling once the temperature $T_1$ is decreased to 1100 °C.

In addition to the roughness measurements, the microstructure of several specimens was examined after testing. Since some of the microstructural features in similar coatings have already been reported [3–5], we address only one particular aspect related to aluminum depletion and gamma-prime formation in the outer coating layer. Unlike the long-term oxidation tests, in which the existing β-(Ni,Pt)Al layer may fully transform into the γ′ phase, the relatively short exposures used in this work produce only a small amount of gamma-prime. The typical microstructure of the coating after 100 one-hour cycles between $T_1 = 1150$ °C and $T_2 = 850$ °C is presented in Fig. 7. In agreement with the previous results [4], the thickness of the outer layer of the coating after cyclic exposure, measured from the string of alumina grit in the mid-section, is about 20% higher than in the as-aluminized condition (Fig. 1). A discontinuous layer of γ′ grains, 5–20 μm in size, is seen next to the interface between the outer layer and the inter-diffusion zone. In addition, a few isolated γ′ grains are located directly underneath alumina scale on the coating surface. Although not visible in the back-scatter electron (BSE) images in Fig. 7, the outer layer of the coating exhibits typical microstructure of the martensitic phase $L1_0$, as reported previously [8,9]. Also indicated in Fig. 7 are occasional inclusions of refractory metals (most likely in the form of a Cr–Re–W–Mo solid solution), small Ta-rich particles at the oxide-metal interface, and grain boundaries in the coating.

The average composition of the outer coating layer after 100 cycles at 1150 °C and the composition of individual phases are listed in Table 1. Despite the significant drop of the average aluminum concentration from about 40% to 30%, the volume fraction of γ′ in the outer portion of the coating after 100 cycles is very small. In this case, a cross-sectional image, such as in Fig. 7, is insufficient to evaluate the amount of γ′ grains in the outer layer. A better estimate can be made using a plain view of the coating (Fig. 8). The specimen in Fig. 8a was polished down to a depth of about 10 μm to remove all traces of alumina scale on the coating surface. The BSE image of the exposed coating, shown in Fig. 8b, was evaluated using image analysis. The volume fraction of gamma-prime, determined from this image, is 1.2%. Subsequent polishing to a greater depth reveals a decrease of the γ′ volume fraction to zero in the mid-section of the coating (about 25 μm from the surface), in agreement with the cross-sectional images in Fig. 7.

In addition to the isolated γ′ grains, thin layers of γ′ phase can be found along grain boundaries of the coating (Fig. 8c and d). The etched surface in Fig. 8(d) also reveals what looks like low-angle boundaries

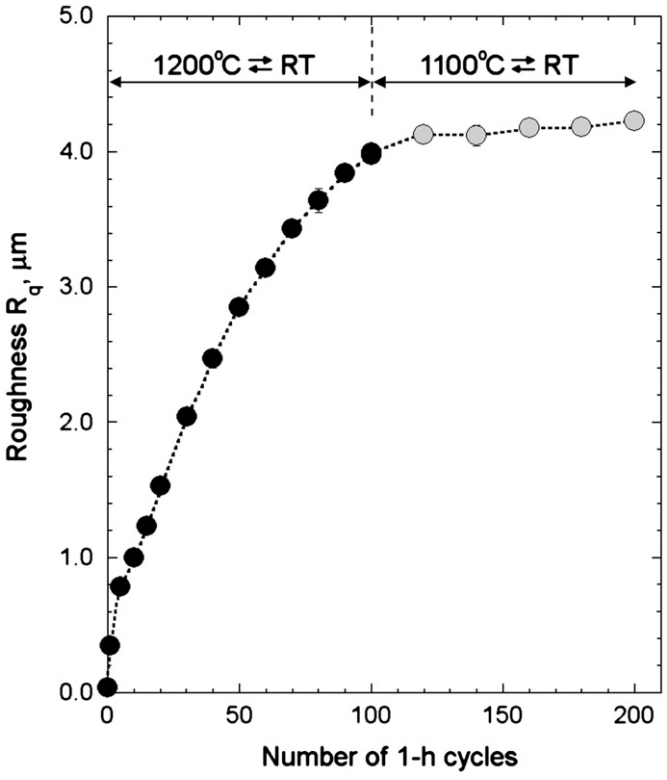


**Fig. 6.** Evolution of rumpling of the (Ni,Pt)Al coating surface with cyclic oxidation between room temperature and 1200 °C for 100 cycles followed by cyclic oxidation between room temperature and 1100 °C. In all cycles, the dwell time at the oxidation temperature was 1 h.

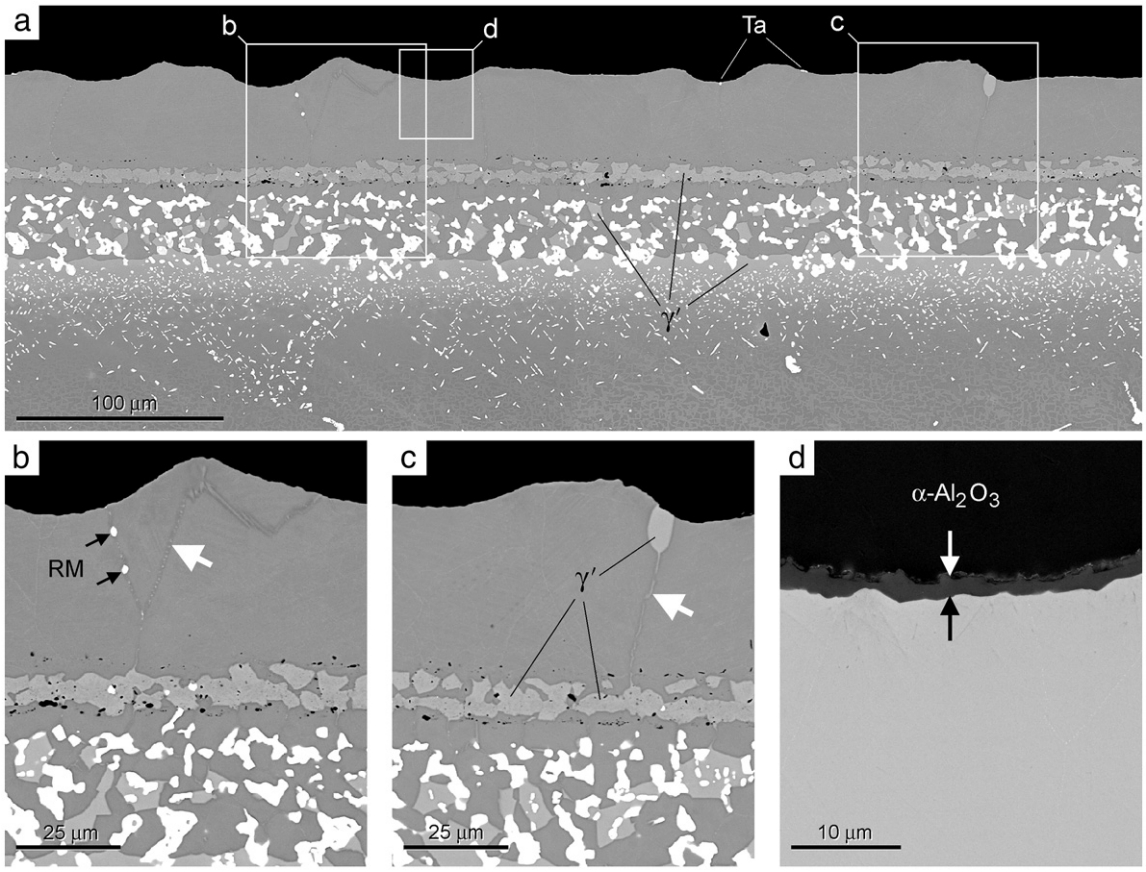


**Fig. 7.** Cross-sectional BSE micrographs showing microstructure of the coating after 100 one-hour cycles between 1150 °C and 850 °C: (a) — general view; (b) and (c) — higher magnification images showing gamma-prime grains, grain boundaries (white arrows) and refractory metal (RM) precipitates indicated by the black arrows in the outer layer of the coating; (d) — 2-μm thick alumina scale on the coating surface. Image contrast in (a), (b), and (c) was set high to reveal compositional difference between the gamma-prime phase and the matrix phase, therefore alumina scale is not discernible on these images.

between smaller domains having different orientation of martensitic plates. These boundaries are decorated with sub-micrometer size precipitates of a Ni-rich phase, possibly $\gamma'$-$Ni_3Al$ or $Ni_5Al_3$. It is interesting to note that no such domains are present in the coating after isothermal oxidation. As previously shown for similar (Ni,Pt)Al coatings after isothermal oxidation at 1150 °C [9], martensite plates within a single grain of the coating have the same orientation. Also, in agreement with our earlier observations [10], no discontinuous $\gamma'$ layer is observed after isothermal oxidation.

## 4. Discussion

The principal result of this work, shown in Fig. 4, indicates that rumpling of the platinum-modified nickel aluminide coatings occurs upon cycling over only 100 degrees, between $T_1 = 1150$ °C and $T_2 = 1050$ °C. Most importantly, decreasing the lower cycle temperature $T_2$ does not produce any further increase of rumpling. These results have important consequences for the relevance of some of the rumpling mechanisms that have been proposed earlier [1,2,8,11]. Three of these mechanisms will be discussed taking into consideration the experimental results described above.

One mechanism relies on the fact that the coating undergoes a martensitic transformation from the nickel-rich $\beta$ phase having B2 cubic structure into the tetragonal $L1_0$ martensite phase during cooling, which is accompanied by a reversible volume change that may enhance rumpling [8,9]. To analyze the role of the $B2 \leftrightarrow L1_0$ transformation, it is useful to consider the Ni-rich side of the binary Ni–Al phase diagram [12] (Fig. 9). The average compositions of the coating in the as-processed condition and after 100 h at 1150 °C are marked (A) and (B), respectively. The equilibrium phase boundaries for the actual coating, which contains Pt, Cr, Co, Ta, etc., are likely to be somewhat different from the binary Ni–Al system. Consequently, the following discussion is merely qualitative and does not refer to a precise chemical composition or a specific cyclic regime. The important feature is that the initial composition of the coating corresponds to the single-phase $\beta$ field at $T_1 = 1150$ °C, whereas it moves into the two-phase $\beta + \gamma'$ field after 100 h, in agreement with the microstructures in Figs. 7 and 8. The relative fractions of the phases in the coating are, of course, different from what can be derived from the phase diagram in Fig. 9.

It is well established that the martensite transformation temperature, $M_s$, depends on composition [13]. For binary Ni–Al alloys, the compositional dependence (in at. %) is described by a straight line from about 60.5Ni–39.5Al ($M_s = -196$ °C) to 69Ni–31Al ($M_s = 927$ °C). This line, labeled $M_s$, is superimposed on the phase diagram in Fig. 9. Such compositional dependence may lead to an erroneous assumption that a Ni-rich coating can also have a very high $M_s$ temperature, for example about 927 °C at 31 at.% Al, or perhaps even higher at lower Al concentrations. However, it is worth noticing that all the binary $\beta$-NiAl alloys in reference [13], having more than 65 at.% Ni, were annealed and quenched from 1400 °C, which is above the $\beta$ solvus curve, to dissolve the second equilibrium phase, $\gamma'$-$Ni_3Al$. The actual aluminide coatings are never exposed to such high temperatures (the incipient melting temperature of the IDZ layer is about 1250 °C) and, hence, they cannot exhibit a monotonic increase of $M_s$ with increasing Ni content, such as shown in Fig. 9. In fact, once the coating composition shifts into the two-phase $\beta + \gamma'$ field (as a result of aluminum depletion due to oxidation and inter-diffusion with the superalloy), the $\beta$ phase composition

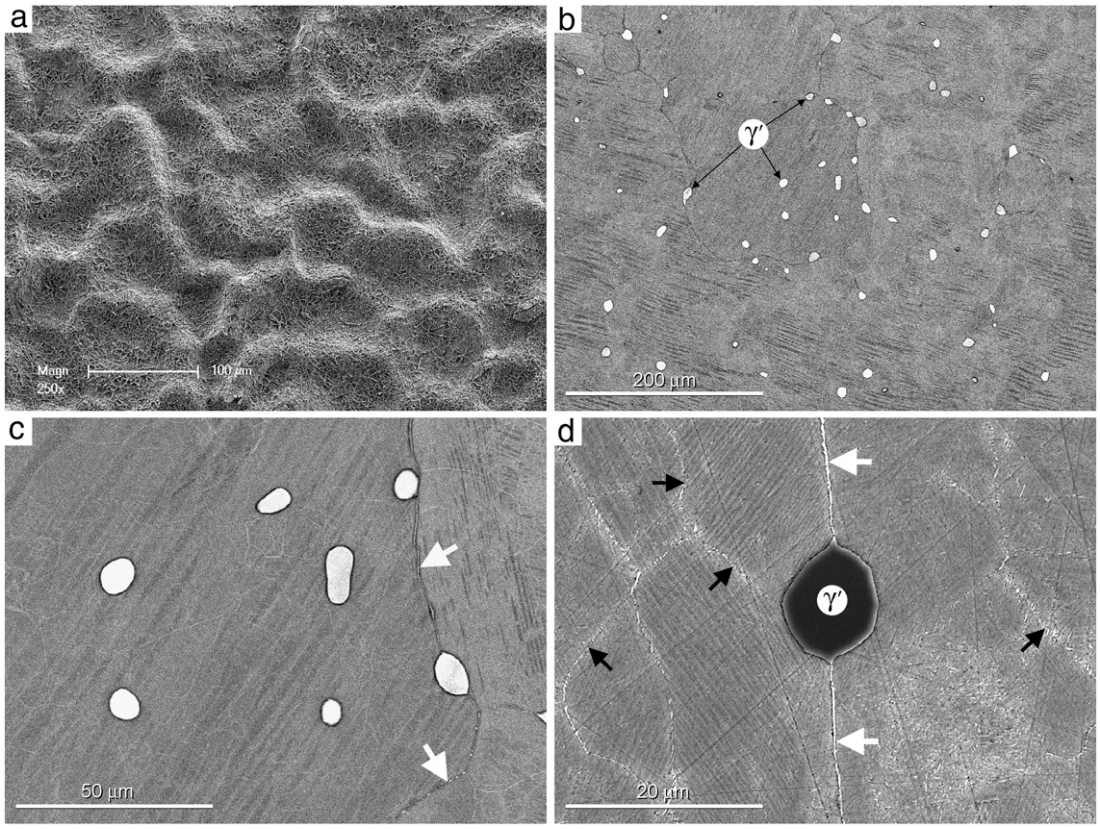


**Fig. 8.** Top view of the coating after 100 one-hour cycles between 1150 °C and $T_2 = 250$ °C: (a) — surface of alumina scale; (b) — microstructure at about 10 μm below the coating surface showing γ′ grains (BSE image); (c) — same area at higher magnification; (d) — same section after etching to reveal martensitic structure, grain boundaries (white arrows) and strings of sub-micrometer particles (black arrows) in the outer layer of the coating (SE image).

becomes constant. This fixed composition is indicated in Fig. 9 by the asterisk at approximately 35.5% Al. Any subsequent exposure at 1150 °C will result in a gradual decrease of the volume fraction of the β phase, but its composition will remain the same, so as its martensite transformation temperature $M_s$. Correspondingly, any further aluminum depletion will increase the amount of the equilibrium γ′ phase. For the binary Ni–Al coating (Fig. 9), the $M_s$ temperature will remain constant at about 320 °C (from the empirical relationship in ref. [13]) for all compositions with less than 35.5 at.% Al. For the (Ni,Pt)Al coating, the fixed composition of the β phase is given in Table 1 (≈30.3 at.% Al). Its martensite transformation temperature can be taken from the DTA results [8] showing $M_s \approx 530$ °C for an aged (i.e., Al-depleted) coating, which had quite similar thermal exposure to the present specimens. In the ternary Ni–Pt–Al or more complex systems, minor changes of the $M_s$ temperature may be expected with concentration of other elements (Cr, Co, Pt) while the overall coating composition remains in the two-phase γ′ field. For example, the concentration of platinum in the β phase should gradually decrease over time, which would result in even lower $M_s$ (platinum is known to increase the martensite transformation temperature [14]).

Some of the model NiPtAl alloys have been shown to exhibit exceptionally high transformation temperatures around 1100 °C [14], but at significantly higher platinum concentrations, ~30 at.% Pt, which is several times higher than in the present coatings. At lower platinum concentrations, comparable with the coating composition, the transformation temperatures were much lower, for example only around 75 °C in the ternary Ni-37%Al-5%Pt alloy [14]. Thus, we can reasonably assume that thermal cycling of the present (Ni,Pt)Al coatings between 1150 °C and $T_2 > 600$–700 °C does not involve any martensitic transformation. This, in turn, suggests that whether the transformation occurs at lower temperatures, or not, has no effect on rumpling because it does not produce any increase of the rumpling

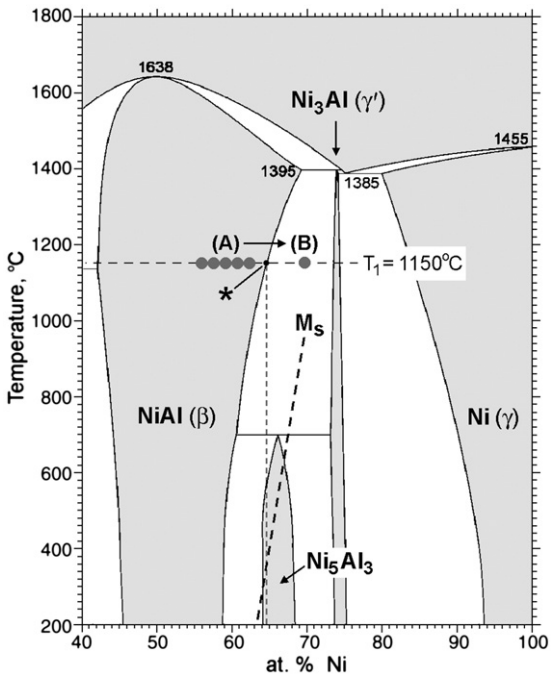


**Fig. 9.** Partial Ni–Al binary phase diagram from reference [12]. Data points (A) and (B) mark the initial composition of the outer coating layer (represented by a range of concentrations) and the average composition after 100 one-hour cycles at 1150 °C, respectively. The asterisk symbol denotes the intersection of the 1150 °C isotherm and the solvus line corresponding to about 35.5 at.% Al for the binary Ni–Al alloy. Concentration dependence of the martensite start temperature, $M_s$, reproduced from reference [13], is superimposed on the phase diagram.

amplitude (Fig. 4). Therefore it may be expected that the transformation-induced strain of the order of 0.7% at $M_s \approx 530$ °C and $A_s \approx 620$ °C [8] is elastic, fully reversible, and does not cause plastic deformation in the (Ni,Pt)Al coatings studied. This does not mean, however, that the transformation has no effect in other aluminide–superalloy systems with different composition. As recent numerical simulations indicate [15], stress in the coating induced by the transformation may be augmented by the thermal mismatch stress (for a certain combination of thermal expansion coefficients) and the cumulative effect of these stresses may exceed yield stress of the coating below $M_s$ and lead to plastic deformation at relatively low temperatures. Again, whether this scenario applies to the present (Ni,Pt)Al coatings or not has no effect of their rumpling behavior.

An additional argument can be put forward taking into account the monotonic increase of the rumpling amplitude with time (Fig. 3). The as-aluminized (Ni,Pt)Al coating does not exhibit martensitic transformation upon cooling to room temperature. The first appearance of the martensitic structure in the coating was detected after 30–40 cycles at 1150 °C, yet the rumpling amplitude increases almost linearly with the number of cycles from the beginning of cyclic oxidation, as shown in Fig. 3. Furthermore, the rumpling mechanism based on the martensitic transformation is inconsistent with the results of the two-stage experiment presented in Fig. 6. Indeed, once the coating composition has reached the level where the $B2 \rightarrow L1_0$ transformation supposedly becomes effective (after the first stage at 1200 °C), the subsequent value of $T_1$ should not make any difference as long as it is above the reverse transformation temperature $A_s$ (and also above ~700 °C to preclude the formation of $Ni_5Al_3$ from the martensite phase). This means that the rumpling should progress at the same rate during the second cycling stage at $T_1 = 1100$ °C. This is clearly not the case since the observed rumpling rate decreases abruptly when oxidation temperature is reduced (Fig. 6). The only alternative is when the $M_s$ and $A_s$ temperatures are precisely between 1100° and 1200 °C, so the transformation takes place during the first cycling stage and does not during the second stage — clearly an unrealistic assumption for the present coatings.

It might be argued that the actual value of the lower cycle temperature above room temperature is irrelevant and that all the rumpling occurs on the final cooling to room temperature. However, as shown in Figs. 3 and 4, both the rumpling amplitude and wavelength are significantly greater after cyclic oxidation than after isothermal oxidation even though the same heating and cooling rates were used for both tests.

Another mechanism proposed to induce rumpling of aluminide coatings is the reversible $\beta \leftrightarrow \gamma'$ phase transformation [11] during heating and cooling. Since this diffusional transformation involves substantial volumetric changes, it might be expected to cause plasticity in the coating upon changing from single-phase $\beta$ to two-phase $\beta + \gamma'$ on cooling and in the opposite direction on heating. In order to assess the viability of this model applied to our aluminide coatings, it should be recognized that the $\gamma'$ grains observed in the coating after 100 one-hour cycles at 1150 °C (Figs. 7 and 8) do not transform to the parent $\beta$ phase on heating and back to gamma-prime on cooling in the next cycle. The size of these grains (5–20 μm) and the spacing between them (tens of micrometers) clearly indicate that they did not precipitate during cooling from 1150 °C, especially at the relatively fast cooling rates used in this work. The same consideration applies to the discontinuous layer of $\gamma'$ at the interface between the outer layer of the coating and the inter-diffusion zone. The only possible route of the formation of these $\gamma'$ grains in the coating is the usual diffusion-controlled phase transformation caused by Al depletion and Ni enrichment *during exposure at 1150 °C*, not during cooling. In other words, the bulky gamma-prime phase observed in the coating at room temperature is the equilibrium "primary" $\gamma'$, which precipitated when the coating composition entered the two-phase $\beta + \gamma'$ field (Fig. 9). This transformation does produce volumetric changes, as noted earlier [10], however it is irreversible and therefore does not generate plastic deformation in each thermal cycle.

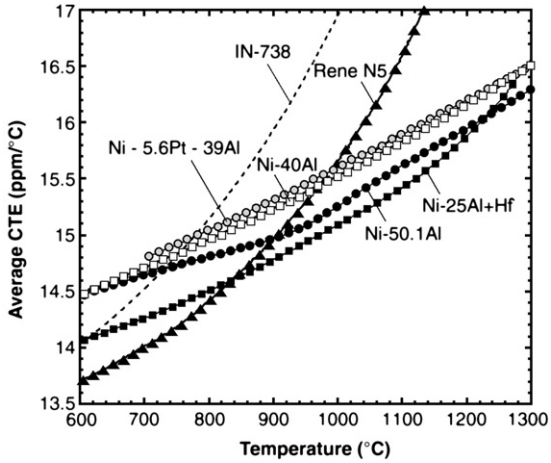


**Fig. 10.** Compilation of thermal expansion data from reference [16] showing the average CTE values for René N5 and several cast aluminides: near-stoichiometric $\beta$-NiAl, nickel-rich $\beta$-NiAl (Ni–40Al), $\gamma'$ phase (Ni − 25Al + Hf) and Ni–5.6Pt–39Al alloy that has similar composition to the (Ni,Pt)Al coatings used in this work (all concentrations are in at. %). All the aluminides have smaller CTE than the superalloy at temperatures above approximately 950°–1000 °C. For comparison, the dashed line shows thermal expansion of IN-738 alloy derived from the manufacturer's data.

As for the "secondary" $\gamma'$ phase that may precipitate according to the $\beta$ phase solvus, its formation is certainly possible. It is probably the $\beta \rightarrow \gamma'$ transformation on cooling that produces the sub-micrometer particles seen in Fig. 8d. Clearly, the beta-phase composition does not follow the equilibrium phase boundary during cooling (otherwise there will be no martensitic transformation). So, cooling from the two-phase $\beta + \gamma'$ field at 1150 °C results in a small amount of secondary $\gamma'$ precipitates, while the remaining supersaturated $\beta$ phase transforms to $L1_0$ martensite. The question is whether the formation of this secondary $\gamma'$ may be responsible for the rumpling of the coating. To address this question, we again invoke the results in Figs. 4 and 6. If the rumpling mechanism relies on the amount of the secondary $\gamma'$ phase precipitating in the coating, then cooling to a lower temperature $T_2$ should precipitate out even more gamma-prime in each cycle, and consequently produce more rumpling. This is clearly not the case (Fig. 4). Furthermore, taking into account the results of the two-stage experiment (Fig. 6), we would have to assume that repeated precipitation–dissolution of the secondary $\gamma'$ occurred exclusively within a narrow temperature interval, specifically between 1150° and 1100 °C, but not at all at lower temperatures. We believe that such an assumption is unrealistic. It is recognized however that, if temperature excursions are performed at a much slower rate, then precipitation of the secondary $\gamma'$ phase may occur according to the equilibrium $\beta/(\beta + \gamma')$ phase boundary. In that case cooling to a lower temperature $T_2$ will cause more gamma-prime to precipitate, induce more plastic strain in the coating and, possibly, result in more rumpling.

Summarizing the discussion, it can be concluded that mechanisms based on either the martensite or the $\beta \leftrightarrow \gamma'$ phase transformations do not provide a viable explanation for the observed rumpling behavior. The present results appear to be consistent with the mechanism, which relies on the thermal mismatch between the coating and the superalloy [1]. One of the original suggestions by Boone et al. [1] was that rumpling might be driven by the coating–substrate CTE mismatch causing plasticity in aluminide coatings. As more CTE results have become available over the recent years, it is now instructive to discuss the actual data.

A compilation of CTE results for various aluminide alloys and René N5 superalloy from reference [16] is presented in Fig. 10. Several important relationships can be derived from these results. First, both binary aluminides, stoichiometric $\beta$-NiAl and $\gamma'$-$Ni_3Al$, have the lowest expansion coefficients at temperatures above ~900 °C. The Ni-rich aluminides, Ni–40Al and Ni–5.6Pt–39Al (at. %), have somewhat higher CTE, and the effect of platinum additions is very small. This means that gradual depletion of a typical low-activity aluminide coating during high

temperature exposure serves to decrease its CTE as more gamma-prime phase develops in the coating. Finally, all the aluminide alloys in Fig. 10 have lower CTE than that of the N5 superalloy at temperatures above 900°–1000 °C. Most importantly, intersection of the CTE curves for René N5 and Ni–5.6Pt–39Al alloy occurs at about 1000 °C. This temperature almost coincides with our highest $T_2 = 1050$ °C, above which most of the rumpling occurs, as shown in Fig. 4. Furthermore, above 1000 °C the CTE mismatch between the superalloy and the platinum–aluminide increases nonlinearly with temperature, which means that the thermal mismatch strain in the coating also increases on cooling from higher temperatures. This is consistent with the substantial increase of the rumpling rate with increasing oxidation temperature $T_1$ (Fig. 6 and ref. [7]).

The fact that rumpling occurs over the same temperature range (above ~1000 °C) that the superalloy CTE is greater than that of the aluminide provides a way to refine the previously described rumpling sequence [3]. At the end of the dwell time at temperature $T_1$ the coating is expected to be stress free (because its creep strength is very low at elevated temperatures [17]). Cooling from $T_1 = 1150$ °C down to about 1000 °C induces a compressive stress in the coating due to the CTE mismatch with the superalloy (Fig. 10). Apparently, some (still undefined) plastic relaxation may occur during this cool down producing plastic strain $\Delta\varepsilon$. Subsequent cooling below 1000 °C causes a reversal of the CTE mismatch. This will first reduce residual compression in the coating and impede further plastic relaxation, and then, at even lower temperatures, induce a tensile mismatch stress. Although not well established, the yield stress of nickel aluminides substantially increases with decreasing temperature below ~650 °C [17]). This freezing out of deformation is probably the reason why no additional plastic relaxation is expected to occur at lower temperatures through the rest of the thermal cycle. Re-heating will create a tensile stress in the coating at temperature $T_1$ that can relax by creep during dwell at $T_1$ producing a plastic strain approximately equal to the cooling plastic strain $\Delta\varepsilon$ as described in more detail elsewhere [3]. Thus, one complete thermal cycle involves two segments when plastic deformation occurs in the coating: the first is in compression on cooling to about 1000 °C and the second is in tension at the beginning of dwell at $T_1$.

One critical element of the CTE mismatch based mechanism pertains to the dwell time at the oxidation temperature, $T_1$. For very short thermal cycles, the dwell time at $T_1$ may be insufficient to reduce compressive stress in the coating to zero. If so, the next cooling cycle will produce smaller $\Delta\varepsilon$ and correspondingly smaller plastic strain during the next dwell, and so on. The result will be a notably smaller rumpling amplitude, for example, after 6-min cycles compared with the same number of one-hour cycles, as indeed was observed previously [3].

Taking into account the CTE results in ref. [16], the thermal mismatch mechanism is also in agreement with the temperature dependence of rumpling. For $T_1 = 1100$ °C, the mismatch strain in the coating upon cooling from 1100° to 1000 °C is quite small, $\Delta\alpha \cdot \Delta T = 7 \cdot 10^{-5}$, whereas for $T_1 = 1200$ °C it is much higher, $\Delta\alpha \cdot \Delta T = 3.4 \cdot 10^{-4}$. This is consistent with the observation that rumpling is barely detected after 100 thermal cycles at 1100 °C but it is very extensive after 100 cycles at 1200 °C [7].

The weak temperature dependence of the rumpling amplitude for different lower cycle temperature, $T_2$, shown in Fig. 4, is probably related to the fact these tests had somewhat different cooling rates (Fig. 2). For instance, cycling between 1150 °C and 950° or 1050 °C leaves longer time for plastic relaxation at elevated temperatures (approaching $T_2$) than cycling between 1150 °C and room temperature.

It is interesting to note that rumpling of platinum–aluminide coatings in the first published report by Boone et al. [1] was quite extensive during cycling at 1100 °C, whereas similar coatings on a second generation single-crystal superalloy were found to rumple much less at this temperature [7]. This difference can be readily understood taking into account that the superalloy used in reference [1] was Inconel IN-738, which has higher thermal expansion coefficient than René N5. The IN-738 CTE curve intersects those for nickel-rich aluminides below 800 °C (Fig. 10), which sets the coating under compression upon cooling down from 1100° to about 800 °C. Correspondingly, the compressive stress and the plastic strain in the coating produced in each thermal cycle by the CTE mismatch are expected to be higher producing more rumpling compared with the lower CTE single-crystal superalloys.

Finally, our results may be of significance in simplifying the task of predicting life of thermal barrier coatings on diffusion aluminide coatings, particularly for complex thermal cycles, for instance those associated with operation of an aircraft engine. Rather than having to model all the time and temperature details of various missions, as prediction codes seek to do, our results indicate that it is only the number of cycles where the temperature exceeds ~1000 °C and the cumulative time above this temperature that affect the aluminide rumpling. For power generation turbines, which are subject to fewer cycles and lower operating temperatures, standard life prediction models [18–20] based simply on the parabolic thickening of the thermally grown oxide may prove to be adequate.

## 5. Conclusions

The results of this work demonstrate that a relatively small temperature decrease in each oxidation cycle, of the order of 100 °C or perhaps even smaller, is sufficient to cause rumpling of the aluminide coating on a second generation superalloy substrate. For a given oxidation temperature, $T_1 = 1150$ °C, the magnitude of rumpling is slightly higher if the lower temperature $T_2$ is in the range from about 750° to 1050 °C than when cooling is performed to room temperature. These observations indicate that neither the martensite nor the $\beta \leftrightarrow \gamma'$ phase transformation occurring during heating and cooling is responsible for rumpling. More likely, rumpling of the diffusion aluminide coating is driven by the thermal expansion mismatch between the aluminide and the underlying superalloy between ~1000° and 1150 °C and facilitated by plastic deformation of the coating and the thermally grown oxide.

## Acknowledgements

The authors are grateful to Mr. K.S. Murphy (Howmet, Whitehall, MI) for providing the specimens, the Office of Naval Research for financial support over the course of this research, and Dr. J.L. Smialek (NASA-Glenn, Cleveland, OH) for valuable comments regarding martensitic transformation in nickel aluminides.

## References

[1] P. Deb, D.H. Boone, T.F. Manley, J. Vac. Sci. Technol., A 5 (6) (1987) 3366.
[2] A.G. Evans, et al., Progr. Mater. Sci. 46 (5) (2001) 505.
[3] V.K. Tolpygo, D.R. Clarke, Acta Mater. 52 (17) (2004) 5115.
[4] V.K. Tolpygo, D.R. Clarke, Acta Mater. 52 (17) (2004) 5129.
[5] V.K. Tolpygo, D.R. Clarke, Acta Mater. 56 (3) (2008) 489.
[6] V.K. Tolpygo, D.R. Clarke, Acta Mater. 52 (3) (2004) 615.
[7] V.K. Tolpygo, D.R. Clarke, Scr. Mater. 57 (7) (2007) 563.
[8] M.W. Chen, et al., Acta Mater. 51 (14) (2003) 4279.
[9] Y. Zhang, et al., Surf. Coat. Technol. 163–164 (2003) 19.
[10] V.K. Tolpygo, D.R. Clarke, Acta Mater. 48 (13) (2000) 3283.
[11] B.A. Pint, S.A. Speakman, C.J. Rawn, Y. Zhang, J. Met. 58 (1) (2006) 47.
[12] M.F. Singleton, J.L. Murray, P. Nash, in: T.B. Massalski (Ed.), 2nd ed, Al–Ni (Aluminum–Nickel), Binary Alloy Phase Diagrams, vol. 1, ASM International, Metals Park, OH, 1990, p. 181.
[13] J.L. Smialek, R.F. Hehemann, Metall. Trans. 4 (6) (1973) 1571.
[14] D.J. Sordelet, et al., Acta Mater. 55 (7) (2007) 2433.
[15] M.L. Glynn, M.W. Chen, K.T. Ramesh, K.J. Hemker, Metall. Mater. Trans., A 35A (2004) 2279.
[16] J.A. Haynes, B.A. Pint, W.D. Porter, I.G. Wright, Mater. High Temp. 21 (2) (2004) 87.
[17] D. Pan, M.W. Chen, P.K. Wright, K.J. Hemker, Acta Mater. 51 (8) (2003) 2205.
[18] R.A. Miller, J. Am. Ceram. Soc. 67 (8) (1984) 517.
[19] T.A. Cruse, S.E. Stewart, M. Ortiz, J. Eng. Gas Turbine Power 110 (1988) 610.
[20] K. Chan, S. Cheruvu, R. Viswanathan, ASME Turbo Expo 2003, ASME, Atlanta, 2003, p. 591.